

On the origin of the marine zinc–silicon correlation

Gregory F. de Souza^{a,*}, Samar P. Khatiwala^b, Mathis P. Hain^c, Susan H. Little^d and Derek Vance^a

^a ETH Zurich, Institute of Geochemistry and Petrology, Clausiusstrasse 25, 8092 Zurich, Switzerland

^b Department of Earth Sciences, University of Oxford, South Parks Road, Oxford OX1 3AN, UK

^cNational Oceanography Centre, University of Southampton, Southampton SO14 3ZH, UK

^dDepartment of Earth Science and Engineering, Imperial College London, London SW7 2AZ, UK

* to whom correspondence should be addressed: ETH Zurich, Institute of Geochemistry and Petrology, NW C83.1, Clausiusstrasse 25, 8092 Zurich, Switzerland; Tel: +41 44 632 6983; E-mail:

Petrology, NW C83.1, Clausiusstrasse 25, 8092 Zurich, Switzerland; Tel: +41 44 632 6983; E-mail:

desouza@erdw.ethz.ch

manuscript in preparation for *Earth and Planetary Science Letters*

Friday, July 21, 2017

Word count: 6873/6500

Abstract

The close linear correlation between the marine distributions of zinc (Zn) and silicon (Si) has puzzled chemical oceanographers since its discovery almost forty years ago, since there is no obvious mechanism of coupling these two nutrient elements. Recent research has shown that such a correlation can be produced in an ocean model without any explicit coupling between Zn and Si, via the export of Zn-rich biogenic particles in the Southern Ocean, consistent with the observation of elevated Zn quotas in Southern Ocean diatoms. Here, we explore the physical and biological mechanisms by which Southern Ocean uptake and export controls the large-scale marine Zn distribution via suites of sensitivity simulations in an ocean general circulation model (OGCM) and a box model. Our simulations focus on the sensitivity of the Zn distribution to the stoichiometry of Zn uptake relative to phosphate (PO_4), drawing directly on observations in culture. Our analysis reveals that OGCM model variants that produce a well-defined step between relatively constant, high Zn: PO_4 uptake ratios in the Southern Ocean and low Zn: PO_4 ratios at lower latitudes fare best in reproducing the marine Zn–Si correlation at both the global and the regional Southern Ocean scale, suggesting the presence of distinct Zn-biogeochemical regimes in the high- and low-latitude oceans that may relate to differences in physiology, ecology or (micro-)nutrient status. Furthermore, a study of the systematics of both the box model and the OGCM reveals that regional Southern Ocean Zn uptake exerts control over the global Zn distribution via its modulation of the biogeochemical characteristics of the surface Southern Ocean. Specifically, model variants with elevated Zn: PO_4 uptake ratios in the Southern Ocean produce near-complete Zn depletion in the Si-poor surface Subantarctic Zone, from which water masses with key roles in the global oceanic circulation are ventilated. By setting the main preformed covariation trend within the ocean interior, the subduction of these Zn- and Si-poor upper-ocean water masses produces a close correlation between the Zn and Si distributions that is barely altered by differential remineralisation during low-latitude cycling.

1. Introduction

As a phytoplankton micronutrient, zinc is a highly versatile element, playing a role as co-factor in metalloenzymes required for biological tasks as varied as carbon fixation (Price and Badger, 1989), gene expression (Twining and Baines, 2013) and possibly the uptake of key macronutrients such as silicon by some phytoplankton groups (Rueter and Morel, 1981; Sherbakova et al., 2005). Indeed, the physiological importance of zinc rivals that of iron (Fe), with more Zn-bearing metalloenzymes known than Fe-bearing ones (Morel et al., 2014). And yet the marine Zn cycle has thus far received limited attention, most likely the result of a long-standing lack of observational data on the abundance of Zn in the sea. The recent efforts of the international GEOTRACES programme have resulted in an order-of-magnitude change in the volume of data available on marine Zn abundance within the last five years (Mawji et al., 2015).

In a recent companion study, Vance et al. (2017) took advantage of this step-change in data availability to study the mechanisms responsible for producing the observed oceanic distribution of Zn. It has been known since the very first reliable analyses of Zn concentration in the ocean (Bruland, 1980) that the Zn distribution mimics that of silicon, a macronutrient that is obligatorily required, and dominantly cycled, by the siliceous phytoplankton known as diatoms. The reasons for the very close, near-linear correlation between these two elements in the ocean has, however, remained unclear for over three decades. A single, direct mechanism, such as the incorporation of Zn into the siliceous frustules of diatoms (Broecker and Peng, 1982), is not permitted by the observation that the Zn content of diatom frustules is orders of magnitude too small to produce the observed relationship between Zn and Si in the ocean (Ellwood and Hunter, 2000). Furthermore, recent cellular-level elemental mapping has revealed that Zn is mostly associated with the organic matter of diatoms (Twining et al., 2004), consistent with its important physiological role, and that cellular Zn is remineralised from sinking diatom detritus at shallow depths together with phosphorus, and not at the greater depths at which siliceous hard parts dissolve (Twining et al., 2014). Thus, the simple correlation between the marine distributions of Zn and Si at the global scale appears at odds with their contrasting biochemical roles and marine biogeochemical behaviour.

Vance et al. (2017) resolved this apparent paradox by drawing on the observation that diatoms in the Southern Ocean have cellular Zn quotas that are 3–15× higher than those of low-latitude phytoplankton (Twining and Baines, 2013). In analogy to the well-established control on the marine Si distribution by the export of Si-rich material from the surface Southern Ocean (Sarmiento et al. 2007), Vance et al. (2017) proposed that strong Zn drawdown in the surface Southern Ocean by diatoms with high Zn quotas is the main control on the global Zn distribution. Their ocean general circulation model (OGCM) results supported this hypothesis by reproducing the observed Zn–Si correlation when Southern Ocean Zn uptake was high, even in the absence of any explicit coupling between the cycles of these two elements. In the view of Vance et al. (2017), the global influence of Southern Ocean uptake is exercised via water masses exported from the Southern Ocean to the global upper and deep ocean, namely Subantarctic Mode Water and Antarctic Intermediate Water (SAMW and AAIW) on the one hand, and Antarctic Bottom Water (AABW) on the other.

In this study, our interest lies in gaining an in-depth understanding of the mechanisms, biological as well as physical, that tie Southern Ocean Zn uptake to the global Zn distribution. Within the context of ocean biogeochemical models in which the cycling of Zn is explicitly tied to that of phosphorus (P), we explore which aspects of biological Zn uptake in the Southern Ocean are most important in establishing its global control, especially considering how this biological uptake interacts with the region’s physical circulation. Our analysis expands upon the modelling work of Vance et al. (2017), complementing them with additional sensitivity simulations that allow a systematic assessment of key controlling processes. The results reveal that regional biological uptake exerts global control on the marine Zn distribution via its influence on the biogeochemical properties of the Southern Ocean’s Subantarctic Zone, from which SAMW and AAIW are subducted. The systematics of the models further suggest that the coupled biological-physical mechanism that ties Southern Ocean uptake of Zn to its global distribution may apply more generally to other biologically-cycled elements in the sea..

2. Methods

2.1. Conceptual approach

We wish to assess the mechanisms by which a correlation between the marine distributions of Zn and Si may come about even in the absence of any explicit coupling between their biogeochemical cycles. We do this in the context of an OGCM, described in more detail below, that simulates the marine biogeochemical cycles of P, Zn and Si. In formulating the biogeochemical model, we were guided by the observations and constraints discussed in Section 1. As a result, our model explicitly couples the marine cycling of Zn to that of P, reflecting observations of Zn uptake in culture, our understanding of the physiological role of Zn as a micronutrient, and direct observation of the Zn distribution within phytoplankton cells (Sunda and Hunstman, 1992; Twining et al., 2004; Twining and Baines, 2013). The simulated surface-ocean uptake of Zn is thus directly tied to that of PO_4 by a stoichiometric parameter $r_{\text{Zn:P}}$, which is the key variable in our sensitivity analysis (see Section 2.2). Additionally, once exported from the surface ocean by sinking particles, Zn is remineralised over the same short length-scale as P, as indicated by observations of remineralising particles (Twining et al., 2014). In contrast, Si uptake in the model is entirely independent of PO_4 uptake, and the length-scale of opal dissolution is greater than that of Zn or P remineralisation, rendering its cycling entirely biogeochemically independent.

2.2. Stoichiometry of simulated Zn uptake

The control parameter in our suite of sensitivity simulations is the stoichiometric parameter $r_{\text{Zn:P}}$, which links the uptake of Zn to the simulated PO_4 uptake. Our parameterisation of $r_{\text{Zn:P}}$ is based on the results of laboratory cultures of three diatom species and two clones of the prymnesiophyte *E. huxleyi* by Sunda and Huntsman (1992). They observed that the Zn:C (and, by extension, Zn:P) ratio of phytoplankton uptake is a non-linear function of the Zn^{2+} concentration of the growth medium, described by an equation of the form:

$$r_{\text{Zn:P}} = \frac{a_{\text{Zn}} \cdot \text{Zn}^{2+}}{b_{\text{Zn}} + \text{Zn}^{2+}} + c_{\text{Zn}} \cdot \text{Zn}^{2+} \quad (\text{Eqn. 1})$$

(I)
(II)

This equation is the linear superposition of a saturating Michaelis-Menten term (I) and a non-saturating linear term (II), which is nicely illustrated by the shape of curves fit to the culture data of Sunda and Huntsman (1992) in Fig. 1a. The species Zn^{2+} represents free aqueous zinc in solution, i.e. Zn that is neither inorganically nor organically complexed. Considering only organic speciation, the concentration of Zn^{2+} in a solution is governed by the total concentration of dissolved Zn on the one hand, and the

concentration (and binding characteristics) of the chelating organic ligand on the other. We assume a globally constant ligand concentration of 1.2 nM, which allows us to circumvent the explicit simulation of Zn complexation chemistry (see Supplementary Information). The assumption of constant ligand concentrations is doubtless an oversimplification; however, the sparse observational dataset shows only relatively limited variability (approximately 0.6–2.4 nM) with no systematic variation (Donat and Bruland, 1990; Bruland, 1989; Ellwood and van den Berg, 2000; Ellwood, 2004; Lohan et al., 2005; Baars and Croot, 2011). This variability in ligand concentrations is small relative to the orders-of-magnitude variability of total dissolved Zn in the ocean.

Parameters a_{Zn} , b_{Zn} and c_{Zn} of Eqn. 1 control different aspects of the dependency of $r_{Zn:P}$ on Zn^{2+} , as illustrated schematically in Fig. 1b. The parameter a_{Zn} determines the maximum asymptotic Zn:P ratio of uptake when the Michaelis-Menten term of Eqn. 1 saturates, whilst b_{Zn} controls the sensitivity of $r_{Zn:P}$ to the presence of Zn^{2+} at low concentrations. The linear parameter c_{Zn} , on the other hand, determines the extent to which the presence of high levels of Zn^{2+} affects $r_{Zn:P}$ beyond the asymptotic Zn:P ratio determined by a_{Zn} . In this paper, we present the results of 24 sensitivity simulations in which the values of these parameters are varied (Table 1). In our base suite of simulations (G1-G11), also presented in Vance et al. (2017), the values of a_{Zn} , b_{Zn} and c_{Zn} are set so as to reproduce the dependence of $r_{Zn:P}$ on Zn^{2+} in the culture data of Sunda and Huntsman (1992), i.e. the curves shown in Fig. 1a (G7-G11), or an approximation thereof in which $r_{Zn:P}$ is a linear function of Zn concentration (G1-G6; see Supplementary Information). We also performed 13 additional sensitivity simulations in which parameters a_{Zn} , b_{Zn} and c_{Zn} are systematically varied within the bounds of the culture data, in order to explore their individual influence on the spatial distribution of $r_{Zn:P}$ and the marine Zn distribution.

2.3. Model framework

OGCM simulations were run on the high-performance cluster *Euler* at ETH Zurich using the transport-matrix method (TMM) of Khatiwala et al. (2005), which allows the efficient offline simulation of passive tracers in the ocean. Here, we use transport matrices derived from MITgcm-2.8, a coarse-resolution version of MITgcm (Marshall et al., 1997) with $2.8^\circ \times 2.8^\circ$ lateral resolution and 15 vertical levels (see Supplementary Information for details). Simulations were carried out with steady annual-

mean circulation fields derived from the equilibrium state of the model after 5000 yr integration. The simulations thus do not include seasonal variability.

Our biogeochemical model of P, Si and Zn cycling is based on the formulation developed for the OCMIP-2 project (Najjar et al., 2007), with simulated uptake of PO_4 and Si in the surface ocean driven by restoring their surface concentrations towards observations in World Ocean Atlas 2013 (Garcia et al., 2013; see Supplementary Information). As discussed in Section 2.2, Zn uptake is directly tied to that of PO_4 by the stoichiometric parameter $r_{\text{Zn:P}}$. Both Zn and P in the implicit particulate export flux are remineralised following a power-law dependency on depth, with an exponent of -0.858 (Martin et al., 1987; Berelson, 2001), whilst regeneration of Si follows an exponential dependency with a length-scale of 1000 m (de Souza et al., 2014). Based on World Ocean Atlas 2013 and literature data, the mean ocean concentrations of PO_4 , Zn and Si are set to values of 2.17 μM , 5.4 nM (Chester and Jickells, 2012), and 92 μM respectively. Biogeochemical model simulations are initialised with these mean ocean concentrations and integrated forward for 5000 model years to steady state.

In addition to the OGCM simulations that are the main focus of this study, we also conducted a suite of 13 sensitivity tests in the 18-box ocean model CYCLOPS (Hain et al., 2014; after Keir, 1988) in which the cycling of Zn is linked to that of PO_4 exactly as in the OGCM simulations. The simplicity of the box model formulation allows us to explicitly prescribe Southern Ocean Zn: PO_4 uptake behaviours and develop a systematic understanding of the response of the large-scale distribution to these changes. As in the OGCM suite, box-model simulations are initialised with constant mean ocean concentrations of PO_4 , Zn and Si as above, and integrated forward for 5000 model years to steady state. Further details are provided in the Supplementary Information.

3. Results & Discussion

3.1. Systematics of base sensitivity simulations

In our base set of simulations (G1-G11), the parameters a_{Zn} , b_{Zn} and c_{Zn} in Eqn. 1 were varied to reproduce the dependency of the Zn: PO_4 uptake ratio $r_{\text{Zn:P}}$ on Zn^{2+} observed in the five culturing experiments of Sunda and Huntsman (1992; Fig. 1). It bears noting here that these simulations are not

meant to represent uptake by a single type of phytoplankton; rather, the culture data are used to constrain the bounds within which the dependency described by Eqn. 1 may vary. Simulations G1-G11 produce what might be called a full spectrum of simulated Zn distributions, ranging from “PO₄-like” (i.e., closely correlated to the simulated PO₄ distribution) to “Si-like”. This is illustrated by the Taylor diagrams in Fig. 2, which quantify the degree of similarity between the three-dimensional Zn distribution and the PO₄ or Si distributions simulated by model variants G1-G11. In these diagrams, symbols that plot closest to the arc representing a normalised standard deviation of 1 and the radial line representing a correlation of 1 (i.e. the “bulls-eye” symbol in Fig. 2) denote the greatest similarity between the two fields being compared. Whilst simulation G1 produces a Zn distribution that mimics that of PO₄ (albeit with elevated surface concentrations), the Zn distribution of simulation G11 is tightly correlated to the model’s distribution of Si, with a normalised standard deviation of ~1 and a correlation coefficient of ~0.97 (Fig. 2a), and the correlation between the simulated fields reproduces the observed Zn–Si relationship in the global ocean (Fig. S3). The exceptional degree of similarity between the Zn and Si fields is illustrated by the depth profiles in Fig. 3a-d, which show basin-average profiles of Zn and Si simulated in G11. As these profiles make amply clear, the difference between the regeneration length-scales of Zn and Si that is built into our model formulation does not result in significant decoupling of their large-scale distributions: the preferential shallow remineralisation of Zn is visible only as a slight enrichment relative to Si within the uppermost 1 km, a feature that does not detract from the close similarity between the two depth profiles in all ocean basins.

The factors controlling the Zn distribution are hinted at by the PO₄ profile included for reference in Fig. 3a: since Zn and PO₄ are regenerated identically in our model, the marked difference between their simulated distributions *must* come about due to differences in their relative uptake in the surface ocean. Indeed, the observed correlation between Zn and Si is best reproduced by simulations in which there is significant meridional variability in the biological Zn:PO₄ uptake ratio $r_{Zn:P}$. This is shown exemplarily for two simulations that vary in their ability to reproduce the observed Zn distribution: in simulation G10 (Fig. 4a), surface Southern Ocean Zn concentrations exceed 1 nM southward of ~40°S, 10° further north than in observations (Zhao et al., 2014); this model also only poorly reproduces the large-scale Zn distribution (Figs. 2 and S4). However, in simulation G11, which produces a Zn distribution closely

correlated to that of Si (Figs. 2 and 3), surface Southern Ocean Zn concentrations decrease more strongly towards the north, with a sharp gradient centred around 47°S in zonal average (Fig. S5a). This strong surface concentration gradient is the result of the uniformly high values of $r_{Zn:P}$ at high southern latitudes, which average ~6 mmol/mol south of 47°S (Figs. 4d and S5b). This step-like behaviour between the low-to-mid-latitudes and the high-latitude ocean is in marked contrast to the slow poleward increase of $r_{Zn:P}$ in simulation G10 (Fig. 4c), in which $r_{Zn:P}$ never exceeds 4 mmol/mol. Thus, in simulation G11, Zn- and nutrient-rich deep waters that upwell to the surface Southern Ocean in the far south experience a consistently strong Zn drawdown as they are transported northwards by the simulated Ekman drift. This sustained elevated Zn drawdown contrasts with simulation G10, in which $r_{Zn:P}$ decreases steadily as Zn-rich surface waters are transported northwards. Analogous differences are visible in the subpolar North Atlantic and North Pacific, whilst in the equatorial Pacific the opposite is true: values of $r_{Zn:P}$ are elevated in simulation G10 relative to G11 (Fig. 4c,d), reflecting the anomalously high surface Zn concentrations there (Fig. 4a).

These results thus show that by simulating the dependence of Zn:PO₄ uptake stoichiometry on ambient Zn²⁺ observed in culture studies, it is possible to reproduce the observed correlation between the large-scale distributions of Zn and Si in the absence of any explicit coupling between the two elements. In the following, we analyse the processes by which this correlation comes about, considering both biological and physical controls: Section 3.2 deals with the role of biological uptake and applies systematic sensitivity simulations to assess the role of the spatial distribution of $r_{Zn:P}$, whilst Sections 3.3 and 3.4 explore the physical mechanism that allows high-latitude uptake to influence the global Zn–Si correlation.

3.2. The role of biology: spatial variability of $r_{Zn:P}$

We have seen in Section 3.1 above that differences in the spatial distribution of $r_{Zn:P}$ appear to be a key variable in determining the global Zn distribution. We now take a more systematic look at the effect of spatial variability in $r_{Zn:P}$, using a suite of 13 sensitivity experiments in which the values of a_{Zn} , b_{Zn} and c_{Zn} are systematically varied within the bounds of the observational constraints provided by the culture data of Sunda and Hunstman (1992; Table 1). A first suite of 9 simulations (G12-G20) revealed that the large-scale Zn distribution is most sensitive to the parameters a_{Zn} and c_{Zn} , whilst its sensitivity to b_{Zn} is

minor (Fig. S6). In the following, we thus focus on the systematics of four sensitivity simulations (G21-G24) in which permutations of the maximum and minimum values of a_{Zn} and c_{Zn} are applied, whilst b_{Zn} remains constant at a mid-range value: for clarity, we refer to the simulations as *aLO-cLO*, *aLO-cHI*, *aHI-cLO*, and *aHI-cHI*. The Taylor diagrams in Fig. 2c,d illustrate the sensitivity of the marine Zn distribution to these permutations – the four simulations span the entire range of behaviours seen in the base set of simulations. From Fig. 2c, it can be seen that low values of both a_{Zn} and c_{Zn} (*aLO-cLO*) produce poor similarity between the Zn and Si distributions. Increasing the value of c_{Zn} (*aLO-cHI*) improves the similarity of the Zn and Si fields, and increasing the value of both parameters leads to a yet greater similarity (*aHI-cHI*). Interestingly, however, when a_{Zn} is high, reducing c_{Zn} to its minimum value results in barely any decrease in the similarity between Zn and Si fields at the global scale (*aHI-cLO*). Thus whilst a high value of c_{Zn} is not sufficient to produce a close similarity between Zn and Si distributions, a high value of a_{Zn} is. In the following, we explore the influence of parameter a_{Zn} in more detail.

Whilst the global metrics in Fig. 2 allow us to quantify the consequences of parameter choices for the marine Zn distribution, they do not allow us to identify the reasons for these changes. In this regard, the surface maps of the Zn:PO₄ uptake ratio $r_{Zn:P}$ shown in Figure 5 are of great utility. These maps reveal that when values of both a_{Zn} and c_{Zn} are low, $r_{Zn:P}$ barely varies between the low and high latitudes (Fig. 5a). Since Zn is also regenerated identically to PO₄ in our model, it follows that the large-scale Zn distribution simulated by *aLO-cLO* is rather similar to the PO₄ distribution (Fig. 2d). In contrast, a high value of one or both of these parameters leads to a meridional gradient in $r_{Zn:P}$ (Fig. 5b-d), although the nature of these gradients is rather different: increasing the value of c_{Zn} produces a relatively slow poleward increase in $r_{Zn:P}$ (Fig. 5b), whilst a high a_{Zn} -value leads to a sharply-defined gradient towards the poles, e.g. around 40°S in the Southern Ocean (Fig. 5c). The sensitivity of $r_{Zn:P}$ to a high a_{Zn} -value is seen most clearly in the Subantarctic Zone (~40-50°S) of the Pacific Ocean (Fig. 5c), where a high a_{Zn} -value elevates $r_{Zn:P}$ relative to simulations with low values of a_{Zn} (Fig. 5a,b). The reason for the different responses of $r_{Zn:P}$ to changes in a_{Zn} and c_{Zn} becomes clear if we recall Eqn. 1 and the effects of parameter changes on the shape of the function as shown in Fig. 1b: parameter a_{Zn} controls the maximum value of $r_{Zn:P}$ in the non-linear, saturating Michaelis-Menten term, whilst parameter c_{Zn} represents the

non-saturating, linear increase of $r_{Zn:P}$ with Zn^{2+} . The effect of a high a_{Zn} -value is thus a strong sensitivity of $r_{Zn:P}$ to even small amounts of Zn^{2+} . This sensitivity produces a sharp poleward shift to high and relatively constant $r_{Zn:P}$ in high-latitude regions, where upwelling of Zn-rich waters leads to elevated Zn^{2+} in the surface. The linear influence of a high c_{Zn} -value, on the other hand, produces a steady poleward gradient of $r_{Zn:P}$, such that $r_{Zn:P}$ varies *within* high-latitude regions, and especially in the Southern Ocean.

The consequence of these differences in the Zn stoichiometry of uptake are clearly seen in the surface distribution of Zn, shown as zonal averages in Fig. 6. If we compare the surface Zn distribution produced by simulations *aLO-cLO* and *aHI-cLO*, it becomes clear that in the Southern Ocean, the main consequence of an elevated a_{Zn} value is a strong southward shift of the Zn gradient between the high- and mid-latitudes. This southward shift is due to the non-linear effect of a_{Zn} discussed above, which produces high $r_{Zn:P}$ uptake ratios even at low Zn^{2+} concentrations, such that Zn continues to be strongly drawn down as Southern Ocean surface waters are transported northwards, even when they become significantly depleted in Zn and Zn^{2+} . It is this persistently high drawdown that leads to the southward shift in the Zn gradient seen in Fig. 6. As a result, Zn concentrations south of 40°S are reduced by over 1nM in *aHI-cLO* relative to *aLO-cLO*, producing a surface Zn distribution that more closely matches the surface Si distribution than that of PO_4 , as shown by the reference curves in Fig. 6: in simulation *aHI-cLO*, the Southern Ocean's Subantarctic Zone, centred around 45°S, is strongly Zn-depleted in contrast to abundant Subantarctic Zn in simulation *aLO-cLO*. Interestingly, the strong stripping out of Zn from the surface Subantarctic zone in simulation *aHI-cLO*, and the similarity of its spatial gradient to that of Si, is consistent with observations in the surface Southern Ocean (Zhao et al., 2014), a fact we shall return to in Section 3.4.

Our sensitivity simulations thus reveal that (a) high values of the parameter a_{Zn} appear to play the most important role in producing a close similarity between the large-scale Zn and Si distributions simulated by our OGCM, and that (b) this parameter also plays an important role in altering the surface Zn distribution in the Southern Ocean, particularly in reducing surface Zn concentrations in the Subantarctic Zone of the Southern Ocean. In other words, a greater similarity between the surface Southern Ocean

distributions of Zn and Si is accompanied by a greater similarity in their global marine distributions, suggesting a link between the two. We investigate this further below.

3.3. Linking regional uptake to global distributions: insights from a box model

A key insight into the manner by which the stoichiometry of regional Southern Ocean Zn uptake exerts influence on the global marine Zn distribution comes from the series of simulations we performed using the 18-box model CYCLOPS (Hain et al., 2014). This sensitivity suite consisted of 13 simulations in which the Zn:PO₄ uptake ratio $r_{Zn:P}$ in the Southern Ocean was prescribed *a priori*. The results illustrate a surprisingly simple systematic behaviour of the surface Southern Ocean, which in the model is represented by two boxes: (a) the Polar Antarctic Zone (PAZ), where deep waters upwell to the surface, and (b) the Subantarctic Zone (SAZ), which is fed from the south by northward-transported Antarctic surface waters, and from which upper-ocean water masses such as SAMW are ventilated. As discussed below, the box-model results indicate that it is the biogeochemical properties of these two regions, and particularly of the Subantarctic Zone, that determine the global Zn–Si and Zn–PO₄ relationships.

Figure 7 illustrates the response of the box-model’s surface Southern Ocean to prescribed changes in the Zn:PO₄ stoichiometry of Southern Ocean uptake. This response is nicely illustrated by the simulated Zn:Si ratio in these surface ocean boxes, which reflects the degree of similarity between the behaviour of Zn and Si in the surface Southern Ocean. As can be seen in Fig. 7, the strongest reaction of surface Zn:Si to changes in the prescribed $r_{Zn:P}$ of Southern Ocean uptake takes place in the SAZ. In the PAZ, the Zn:Si ratio is relatively insensitive to changes in Southern Ocean $r_{Zn:P}$, being closely buffered towards the deep-ocean value by the upwelling of deep waters (Fig. 7a). In contrast, the Zn:Si ratio of the Subantarctic surface varies considerably with $r_{Zn:P}$: when Zn uptake is limited by low values of $r_{Zn:P}$, the Zn:Si ratio of surface waters rises as they are transported northwards into the SAZ, since Si is taken up more rapidly than Zn. When $r_{Zn:P}$ is high, however, the uptake of Zn keeps pace with the strong stripping out of Si from the Southern Ocean surface, thus preventing the Zn:Si ratio of surface waters from rising as they are transported northwards from the Antarctic, and leading to a SAZ that is both Zn- and Si-depleted. This concomitant depletion of Zn and Si leads to only minor variation in Zn:Si ratios in the surface Southern Ocean: as can be seen in Fig. 7a, at $r_{Zn:P}$ values of above ~5mmol/mol, the

Subantarctic Zn:Si ratio is very similar to the global-ocean mean value that also characterises the PAZ. Figure 7b shows that it is these same simulations – with high Southern Ocean $r_{Zn:P}$ and Zn-depleted Subantarctic waters – that show the closest linear correlation between the simulated global-ocean distributions of Zn and Si, as reflected by correlation coefficients close to unity. Since the $r_{Zn:P}$ of Southern Ocean uptake is the only parameter that varies between these simulations, and the model’s main response is in the surface Subantarctic Zone, these results strongly suggest that Southern Ocean uptake exerts its control on the global Zn–Si relationship via its modulation of Subantarctic Zn status.

The intuition gained from analysis of the box-model systematics can be directly applied to our OGCM simulations. The right-hand panels of Fig. 7 show results for simulations G1-11 and G21-24 analogous to those presented for the box model in Fig. 7a,b. From Fig. 7c, it is clear that here too, an increase in $r_{Zn:P}$ in the Southern Ocean leads to a strong decrease in the Zn:Si ratio of the SAZ (unlike the box model, Antarctic Zn:Si also responds to $r_{Zn:P}$, albeit less sensitively). Simulations in which Southern Ocean $r_{Zn:P}$ values are low produce a Subantarctic surface that is highly enriched in Zn relative to Si; in Fig. 7d, it can be seen that these simulations also fare worst in reproducing the global Zn–Si correlation, with high normalised root-mean-square (RMS) differences between their simulated Zn and Si distributions. On the other hand, as in the box-model, simulations in which high $r_{Zn:P}$ values lead to a Subantarctic Zn:Si ratio close to the mean-ocean value (Fig. 7c) produce the best match between the Zn and Si fields (Fig. 7d). Figure 8 illustrates this exemplarily for the simulations G10 and G11, previously considered in Section 3.1. In simulation G10, the low Zn:PO₄ ratio of Southern Ocean uptake (Fig. 4c) limits the degree to which Zn is drawn down from surface waters, such that the Zn:Si ratio of the Southern Ocean surface increases northwards, with a zonal band of elevated Zn:Si centred in the SAZ (Fig. 8a). In contrast, the elevated Southern Ocean Zn uptake in simulation G11 (Fig. 4d) leads to a near-constant surface Zn:Si ratio in the Southern Ocean (Fig. 8b), since Zn and Si are similarly rapidly stripped from the surface. This simulation also produces the closest correlation between global Zn and Si distributions (Fig. 3).

The Southern Ocean’s Subantarctic Zone is the formation region for upper-ocean water masses of near-global importance, playing a key role in the ventilation of the basal-thermocline and intermediate ocean by SAMW and AAIW (e.g. Hanawa and Talley, 2001; Sallée et al., 2010). The most likely physical

mechanism for translating the regional signal of Zn uptake to the scale of the global marine Zn distribution is thus the subduction and circulation of SAMW/AAIW, transposing the low- Zn, low-Si signature of the surface Subantarctic Zone into the ocean interior. Indeed, in our OGCM simulations, the Zn:Si ratio along an isopycnal corresponding to SAMW in the Atlantic Ocean ($\sigma_\theta = 26.8 \text{ kg/m}^3$), which outcrops in the Subantarctic zone around 45°S in the OGCM, responds sensitively to the $r_{\text{Zn:P}}$ value of Southern Ocean uptake: as with the Subantarctic surface from which it is ventilated, the Zn:Si ratio on this isopycnal falls to values close the mean-ocean ratio with elevated Southern Ocean Zn uptake. It also correlates exceptionally strongly with the RMS difference between the large-scale Zn and Si distributions ($r^2 = 0.99$; Fig. S7): the marine Zn and Si distributions are most similar when the Zn:Si ratio on this isopycnal is closest to the mean-ocean ratio. Taken together, these interrelationships show that the biogeochemical properties of the upper-ocean water masses ventilated from the surface Subantarctic Zone are the decisive element in creating a close correlation between the global marine Zn and Si distributions.

3.4. General systematics of the Subantarctic control

The discussion in Sections 3.2 and 3.3 above has clearly shown the importance of Subantarctic surface properties for the global Zn distribution, and the physical mechanism by which this control comes about. We now attempt to gain a more generalised understanding of the Subantarctic control on the large-scale distribution of Zn and biologically-cycled elements in general.

We first consider the biological drawdown of Zn and PO_4 in the surface Southern Ocean. The results discussed above have shown that Zn-depletion in the surface Subantarctic is key to reproducing the observed Zn–Si correlation. We apply a simple generalised framework to assess the relative Southern Ocean drawdown of Zn and PO_4 simulated by our sensitivity suite. Here, we build upon the fact that PO_4 concentrations in the Subantarctic Zone are only ~40% of those in Antarctic waters south of the Polar Front (Garcia et al., 2013 – *suggestion for a better ref, Mathis?*). If we make the simplifying assumption that all nutrient supply to the Subantarctic surface comes through Ekman transport from the south, then in order to produce a Subantarctic surface ocean depleted in Zn, Southern Ocean Zn drawdown must be sufficiently strong to produce Zn-depletion when PO_4 has been drawn down to only

40% of its initial Antarctic value. We thus calculate the expected relationship between the drawdown of Zn and PO₄ that results from the parameter choices for the equation governing $r_{Zn:P}$ (Eqn. 1) in our OGCM sensitivity suite; the results are shown in Fig. 9. Here, it can be seen that when PO₄ has been drawn down to 40% of its initial Antarctic concentration, the fraction of residual Zn varies between ~0% and ~60% depending on the simulation. Those simulations that draw down Zn most strongly, depleting Zn when residual PO₄ is at 40% or more, correspond best to the observed covariation between Zn and PO₄ in the surface Southern Ocean (Zhao et al., 2014; Fig. 9). Tellingly, it is these same simulations (G11, *aHI-cLO*, *aHI-cHI*) that best reproduce the global linear relationship between Zn and Si (Fig. 2). This general framework thus shows that a key variable in determining Subantarctic Zn status, and thus the large-scale Zn distribution, is the *integrated* Zn:PO₄ uptake ratio experienced by surface Southern Ocean water masses as they are transported northwards to the Subantarctic Zone.

Secondly, whilst in the case of Zn it is *depletion* in the Subantarctic surface that is a key prerequisite to correctly simulating the Zn–Si and Zn–PO₄ relationships, the systematics of our box-model simulations offer the tantalising suggestion that this might be only a specific case of a coupled biological-physical Subantarctic mechanism that explains elemental correlations in the sea more generally. As discussed in Section 3.3, box-model simulations in which high $r_{Zn:P}$ values lead to strong Zn drawdown have a Subantarctic Zn:Si ratio very similar to the global-ocean mean (Fig. 7a), and strongly correlated Zn and Si distributions. Analysis of the Zn:PO₄ systematics of these simulations (Fig. S8) shows that the simulated Zn distribution becomes, instead, almost perfectly linearly correlated with the PO₄ distribution when the Zn:PO₄ ratio in the Subantarctic Zone equals the mean-ocean Zn:PO₄ ratio of ~2.5 mmol/mol. The analogous existence of such a link between Subantarctic elemental stoichiometry and global distributions for both Zn–Si and Zn–PO₄ suggests a more general mechanism of Subantarctic control. The ventilation of upper-ocean water masses from the Subantarctic introduces its surface stoichiometric signal into the ocean interior, setting the preformed stoichiometry of the upper ocean (Fig. 10). If this upper ocean “endmember”, with low elemental concentrations, bears the same stoichiometric ratio between two elements as the nutrient-rich deep ocean that influences the global mean, the global relationship between these two elements will be near-linear (Fig. 10), as in the case of Zn and Si in the modern ocean. In contrast, if Southern Ocean uptake leads to a strong relative depletion in one of these

elements in the Subantarctic surface, the low-concentration endmember subducted from the Subantarctic will bear a lower elemental ratio than the nutrient-rich deep ocean, and the global relationship between the two elements will be convex-upwards (Fig. 10), with a steep relationship representing mixing between Subantarctic-sourced waters and the nutrient-rich deep ocean – as in the case of Zn and PO₄ in the modern ocean (Fig. S3) or, indeed, Si and PO₄.

3.5. Synthesis and broader implications

The results discussed above have highlighted the extent to which Southern Ocean Zn uptake plays a role in determining the global Zn distribution. Specifically, the OGCM results presented in Section 3.2 show that the extension of elevated Zn uptake into the Subantarctic Zone, even as Zn and Zn²⁺ concentrations drop, is key to reproducing the observed large-scale Zn–Si correlation (Fig. 4). It must be noted that our biogeochemical model achieves this uptake via a relationship between Zn:PO₄ uptake ratios and Zn²⁺ (Eqn. 1) that is certainly an oversimplification of the complexity of marine Zn biogeochemistry (e.g. Varela et al., 2011). Additionally, the specifics of our results (such as the numerical values of optimal coefficients) are also dependent on our choice of the concentration of the chelating ligand that binds most dissolved Zn. Nonetheless, the sensitivity approach we employ in this study allows us to identify macro-scale biogeochemical processes that are associated with the simulation of a more realistic marine Zn distribution, and it is on this process understanding that we focus here. The box-model and OGCM results in Section 3.3 (Fig. 7) and the general frameworks presented in Section 3.4 (Figs. 9,10) reveal the combination of biological and physical processes that link Southern Ocean uptake to the global marine Zn distribution, via the Subantarctic surface.

Whilst at the global scale the production of a Zn-depleted Subantarctic surface would appear to be a sufficient condition for reproducing the Zn distribution, at the regional scale additional nuances appear. Simulations *aHI-cLO* and *aHI-CHI*, for instance, demonstrate similar global skill (Fig. 2c,d), and both produce a Zn-depleted Subantarctic surface, although Zn drawdown in *aHI-CHI* is considerably stronger than in *aHI-cLO* (Fig. 9a), as a result of the extremely high $r_{Zn:P}$ of uptake that *aHI-CHI* simulates at high Zn concentrations (Fig. 9b). This elevated Zn uptake has consequences for the latitudinal distribution of Zn in the surface Southern Ocean simulated by *aHI-CHI*, limiting the degree to which Zn concentrations can rise in regions of Southern Ocean upwelling centred around 60°S (Fig. 6). Thus

unlike *aHI-cLO*, which reproduces the observed surface Southern Ocean covariation between Zn and Si along the prime meridian (Zhao et al., 2014) with good fidelity, *aHI-cHI* consistently underestimates Zn concentrations in the far south (Fig. S9). This difference in regional skill suggests that the step-like increase in the $r_{Zn:P}$ of uptake simulated by *aHI-cLO*, with low values in the temperate latitudes and a rapid rise to a plateau of high $r_{Zn:P}$ values in the subpolar and polar oceans, better captures the variation of $r_{Zn:P}$ required to explain the Zn distribution at multiple scales ranging from the regional to the global. Our biogeochemical model produces this step via what is essentially a physiological mechanism (Eqn. 1), but the sharp separation of oceanic provinces that results suggests the possibility that such a variation might, in the real ocean, be driven instead by differences in biogeography or nutrient status.

Differing Zn quotas in high- and low-latitude phytoplankton could, for instance, be the result of adaptive changes to ambient Zn concentrations within phytoplankton groups, analogous to differences in Si quota observed between high-latitude and equatorial diatoms (e.g. Baines et al., 2010); such an adaptation is indeed suggested by the lower Zn requirements observed in open-ocean phytoplankton species relative to coastal ones (Sunda and Huntsman, 1992). Alternatively, elevated Zn quotas in high-latitude high-nutrient low-chlorophyll regions such as the Southern Ocean and subpolar North Pacific may be a biochemical response to the chronic iron limitation of phytoplankton in these regions (Chisholm and Morel, 1991), since iron limitation has been shown to elevate Zn quotas in natural iron-limited phytoplankton communities (Cullen et al., 2003). Our biogeochemical model is agnostic as to the specific causes of the variation in $r_{Zn:P}$. What is clear is that model variants that produce a realistic Zn distribution also reproduce the marked difference in Zn quotas observed between Southern Ocean diatoms and low-latitude genera (Twining and Baines, 2013). In our opinion, this result strongly suggests that it is Southern Ocean diatoms that are dominantly responsible for the large-scale Zn-Si correlation in the global ocean, and that – via their extraordinary affinity for Zn and abundant seasonal blooms – they dominantly control the fluxes driving the global-scale Zn cycle. Certainly, in our most skilful model variants, Zn export fluxes south of 40°S represent 44% or more of global Zn export (Table S2), making the Southern Ocean almost as important for Zn as for Si (54%), and more than twice as important as for the export of P (19%).

The far-reaching consequences of elevated Southern Ocean Zn uptake are highlighted by the fact that the physical model we employ simulates significant low-latitude upwelling (Resplandy et al., 2016). This upwelling is patently insufficient to overcome the Zn depletion of the upper ocean that results when Zn is stripped out of the Subantarctic surface ocean. With most Zn efficiently trapped within the deep Southern Ocean by the elevated Zn export fluxes there, wind-driven upwelling in coastal and equatorial regions can only tap into a relatively small Zn upper-ocean pool, most of which likely is efficiently recycled within the upper ocean due to the shallow remineralisation of organic-associated Zn (Twining et al., 2014). It would thus seem that the low-latitude cycling of Zn is most likely conducted within a shallow recycling loop that remains rather disconnected from the large-scale, Southern-Ocean-dominated cycle determining the global Zn distribution. This raises the interesting possibility that the observed differences between the Zn quotas of eukaryotic and prokaryotic phytoplankton may also be the consequence of adaptation to ambient Zn concentrations, rather than representing a fundamental physiological difference: by sequestering Zn in the deep Southern Ocean, high-latitude eukaryotic diatom communities might effectively “starve” low-latitude phytoplankton communities, including prokaryotic cyanobacteria that thrive in the subtropics, of zinc. Whilst speculative, it appears at least possible that the lower Zn quotas observed for low-latitude cyanobacteria (e.g. Twining et al., 2011) might represent an adaptive response to this diatom-driven Zn starvation, rather than reflecting a fundamental difference in physiological demand between prokaryotes and eukaryotes (cf. Saito et al., 2003).

At the broadest scale, the correlative mechanism identified by this study has applicability beyond the marine Zn distribution. As discussed in detail in Section 3.4, the degree to which Southern Ocean uptake draws down the Subantarctic concentration of an element relative to that of PO_4 determines the upper-ocean endmember that defines the interior-ocean correlation between that element and PO_4 (Fig. 10). This mechanism should apply equally to other elements whose oceanic residence time is sufficiently long for large-scale circulation to play a significant role in determining their distribution. In this context, the much-discussed “kink” in the marine relationship between cadmium (Cd) and PO_4 would appear to result from Southern Ocean uptake that is elevated in Cd relative to PO_4 , albeit to a smaller extent than is the case for Zn (cf. Baars et al., 2014). Further observations of *in situ* utilisation and phytoplankton

stoichiometry, as well as modelling studies of their effects on the large-scale distribution, would allow a robust test of this hypothesis.

4. Conclusions

In this study, our interest has been to understand the key mechanisms that govern the global marine Zn distribution, and particularly its close similarity to that of Si, in the face of its close mechanistic links to the cycling of PO₄. Our sensitivity suites have shown that the marked similarity between Zn and Si is driven by the stoichiometry of Zn uptake relative to that of PO₄, via its influence on the elemental stoichiometry of the surface ocean, and particularly that of the Subantarctic zone of the Southern Ocean, where water masses that fill the upper ocean are formed: when Zn is drawn down strongly from surface Southern Ocean waters, the variability in the Zn:Si ratio of the surface Southern Ocean is markedly damped, bringing the Zn:Si ratio subducted into the upper-ocean interior by SAMW/AAIW close to that of the whole-ocean mean. This similarity in preformed Zn:Si ratios leads to a similarity between the large-scale distributions of the two elements that cannot be undone by differences in the depths at which they are remineralised from sinking biogenic particles.

Acknowledgements

GFdS is supported by a Marie Skłodowska-Curie Research Fellowship under EU Horizon2020 (SOSiC; GA #708407).

References

- Baars, O., Abouchami, W., Galer, S.J.G., Boye, M., Croot, P.L., 2014. Dissolved cadmium in the Southern Ocean: distribution, speciation, and relation to phosphate. *Limnol. Oceanogr.* 59, 385-399.
- Baines, S.B., Twining, B.S., Brzezinski, M.A., Nelson, D.M., Fisher, N.S., 2010. Causes and biogeochemical implications of regional differences in silicification of marine diatoms. *Glob. Biogeochem. Cyc.* 24, GB4031, doi: 10.1029/2010gb003856.
- Broecker, W.S., Peng, T.H., 1982. *Tracers in the Sea*. Eldigio Press/Lamont-Doherty Geological Observatory, Palisades, NY.
- Bruland, K.W., 1980. Oceanographic distributions of cadmium, zinc, nickel, and copper in the North Pacific. *Earth Planet. Sci. Lett.* 47, 176-198.

510 Chisholm, S.W., Morel, F.M.M., 1991. Special Issue: What controls phytoplankton production in
 511 nutrient-rich areas of the open sea? *Limnol. Oceanogr.* 36, 1507-1970.
 512 Ellwood, M.J., Hunter, K.A., 2000. The incorporation of zinc and iron into the frustule of the marine
 513 diatom *Thalassiosira pseudonana*. *Limnol. Oceanogr.* 45, 1517-1524.
 514 Hain, M.P., Sigman, D.M., Haug, G.H., 2014. Distinct roles of the Southern Ocean and North Atlantic
 515 in the deglacial atmospheric radiocarbon decline. *Earth Planet. Sci. Lett.* 394, 198-208.
 516 Keir, R.S., 1988. On the Late Pleistocene ocean geochemistry and circulation. *Paleoceanogr.* 3, 413-
 517 455.
 518 Khatiwala, S., Visbeck, M., Cane, M.A., 2005. Accelerated simulation of passive tracers in ocean
 519 circulation models. *Oc. Modell.* 9, 51-69.
 520 Marshall, J., Adcroft, A., Hill, C., Perelman, L., Heisey, C., 1997. A finite-volume, incompressible
 521 Navier-Stokes model for studies of the ocean on parallel computers. *J. Geophys. Res. Ocean.* 102,
 522 5733-5752.
 523 Mawji, E., Schlitzer, R., Dodas, E.M., Abadie, C., Abouchami, W., Anderson, R.F., et al., 2015. The
 524 GEOTRACES Intermediate Data Product 2014. *Mar. Chem.* 177, 1-8.
 525 Resplandy, L., Keeling, R.F., Stephens, B.B., Bent, J.D., Jacobson, A., Rödenbeck, C., Khatiwala, S.,
 526 2016. Constraints on oceanic meridional heat transport from combined measurements of oxygen and
 527 carbon. *Clim. Dyn.* 47, 3335-3357.
 528 Rueter, J.G., Morel, F.M.M., 1981. The interaction between zinc deficiency and copper toxicity as it
 529 affects the silicic acid uptake mechanisms in *Thalassiosira pseudonana*. *Limnol. Oceanogr.* 26, 67-
 530 73.
 531 Saito, M.A., Sigman, D.M., Morel, F.M.M., 2003. The bioinorganic chemistry of the ancient ocean: the
 532 co-evolution of cyanobacterial metal requirements and biogeochemical cycles at the Archean-
 533 Proterozoic boundary. *Inorg. Chim. Acta* 356, 308-318.
 534 Sallée, J.-B., Speer, K., Rintoul, S., Wijffels, S., 2010. Southern Ocean thermocline ventilation. *J. Phys.*
 535 *Oceanogr.* 40, 509-529.
 536 Sarmiento, J.L., Gruber, N., Brzezinski, M.A., Dunne, J.P., 2004. High-latitude controls of thermocline
 537 nutrients and low latitude biological productivity. *Nature* 427, 56-60.
 538 Sarmiento, J.L., Simeon, J., Gnanadesikan, A., Gruber, N., Key, R.M., Schlitzer, R., 2007. Deep ocean
 539 biogeochemistry of silicic acid and nitrate. *Glob. Biogeochem. Cyc.* 21, doi:
 540 10.1029/2006GB002720.
 541 Sherbakova, T.A., Masyukova, Y.A., Safonova, T.A., Petrova, D.P., Vereshagin, A.L., Minaeva, T.V.,
 542 et al., 2005. Conserved motif CMLD in silicic acid transport proteins of diatoms. *Mol. Biol.* 39, 269-
 543 280.
 544 Sigman, D.M., DiFiore, P.J., Hain, M.P., Deutsch, C., Wang, Y., Karl, D.M., et al., 2009. The dual
 545 isotopes of deep nitrogen as a constraint on the cycle and budget of oceanic fixed nitrogen. *Deep-*
 546 *Sea Res. I* 56, 1419-1439.

- Sunda, W.G., Huntsman, S.A., 1992. Feedback interactions between zinc and phytoplankton in seawater. *Limnol. Oceanogr.* 37, 25-40.
- Twining, B.S., Baines, S.B., Fisher, N.S., 2004. Element stoichiometries of individual plankton cells collected during the Southern Ocean Iron Experiment (SOFEX). *Limnol. Oceanogr.* 49, 2115-2128.
- Twining, B.S., Baines, S.B., Bozard, J.B., Vogt, S., Walker, E.A., Nelson, D.M., 2011. Metal quotas of plankton in the equatorial Pacific Ocean. *Deep-Sea Res. II* 58, 325-341.
- Twining, B.S., Baines, S.B., 2013. The trace metal composition of marine phytoplankton. *Ann. Rev. Mar. Sci.* 5, 191-215.
- Twining, B.S., Nodder, S.D., King, A.L., Hutchins, D.A., LeClerc, G.R., DeBruyn, J.M., et al., 2014. Differential remineralization of major and trace elements in sinking diatoms. *Limnol. Oceanogr.* 59, 689-704.
- Vance, D., Little, S.H., de Souza, G.F., Khatiwala, S., Lohan, M.C., Middag, R., 2017. Silicon and zinc biogeochemical cycles coupled through the Southern Ocean. *Nature Geosci.*, doi: 10.1038/ngeo2890.
- Varela, D.E., Willers, V., Crawford, D.W., 2011. Effect of zinc availability on growth, morphology, and nutrient incorporation in a coastal and an oceanic diatom. *J. Phycol.* 47, 302-312.
- Zhao, Y., Vance, D., Abouchami, W., de Baar, H.J.W., 2014. Biogeochemical cycling of zinc and its isotopes in the Southern Ocean. *Geochim. Cosmochim. Acta* 125, 653-672.

Figures

Fig. 1: Stoichiometry of simulated uptake. Panel *a* shows the dependence of the Zn:P uptake ratio $r_{\text{Zn:P}}$ on the ambient concentration of Zn^{2+} observed in culture experiments by Sunda and Huntsman (1992). Data in Sunda and Huntsman (given as Zn:C ratios) have been converted to Zn:P using the Redfield C:P ratio of 106 mol/mol. Panel *b* schematically illustrates the influence of the parameters a_{Zn} , b_{Zn} and c_{Zn} in Eqn. 1 on the shape of this dependency.

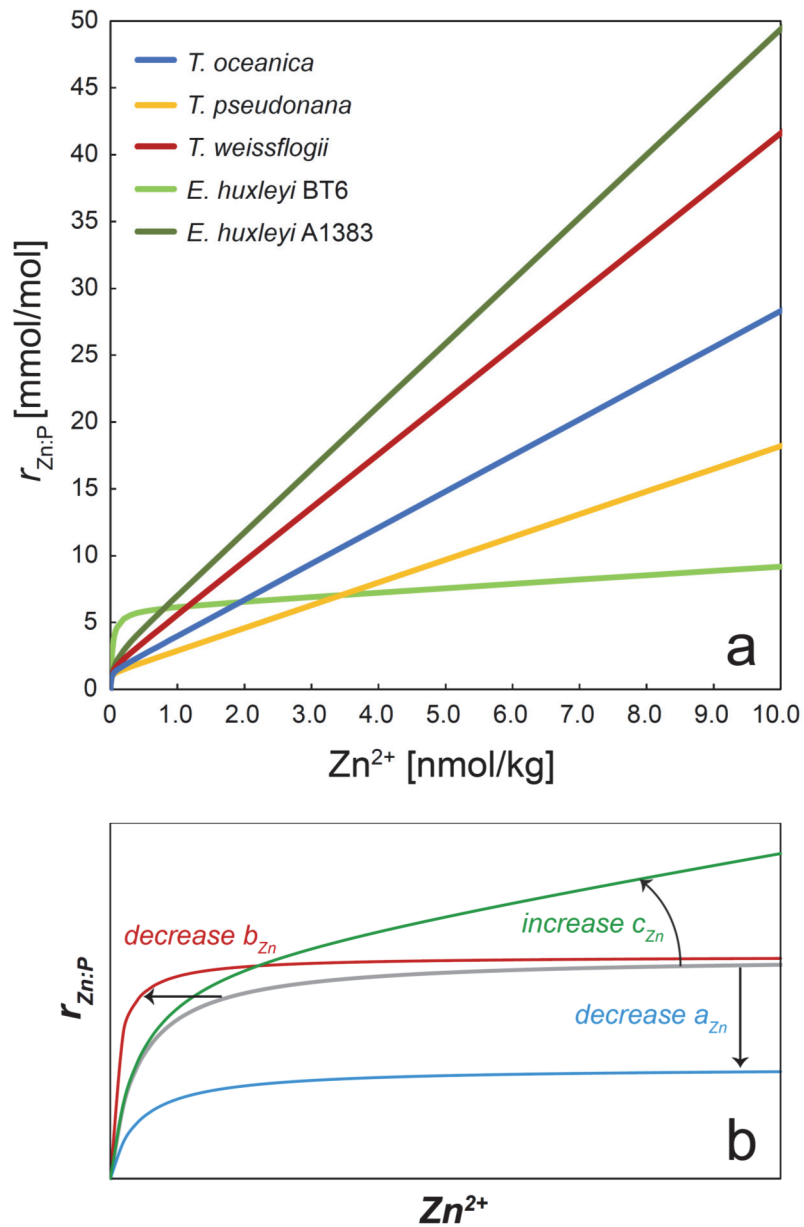


Fig. 2: Taylor diagrams illustrating the degree of similarity between the simulated Zn field and (a,c) the simulated Si field or (b,d) the simulated PO₄ field. Upper panels show results for the base set of simulations G1-G11; lower panels show results for the simulations G21-G24 (simulations G9 and G11 are included as reference). The pink star in panel *b* represents the similarity between simulated Si and PO₄ fields for reference. The bulls-eye symbol at (1,1) represents the point at which both fields being compared are statistically identical.

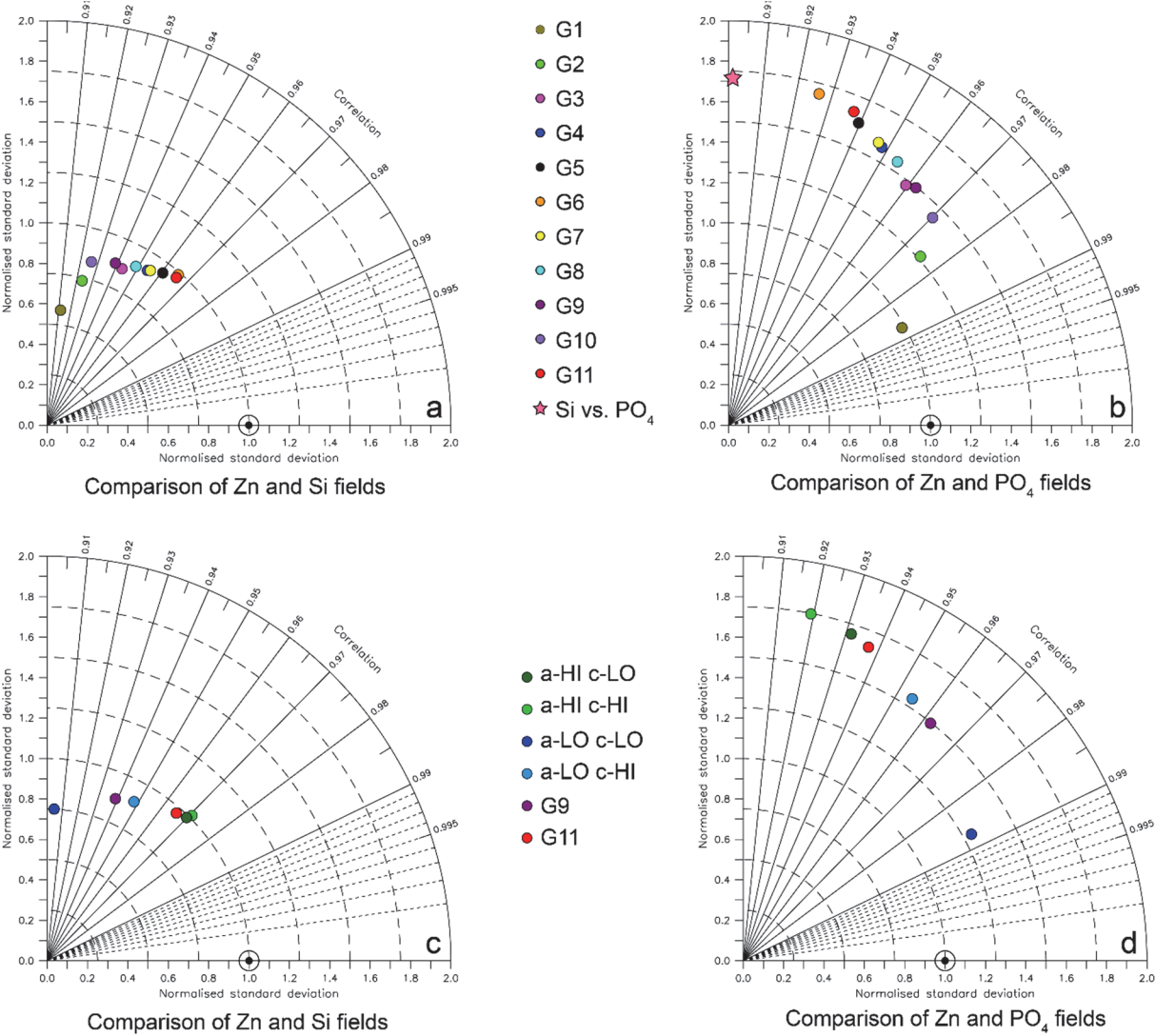


Fig. 3: Basin-average depth profiles produced by (a-d) simulation G11, in which the global Zn–Si relationship is well reproduced. The preferential shallow remineralisation of Zn is visible in all profiles, but only as a relatively minor shoaling of the Zn-cline relative to the silicicline. In panel *a*, the basin-average PO_4 profile for the Atlantic basin is also shown, in order to show the degree of difference between the Zn and PO_4 fields, despite the fact that our model couples their uptake and regeneration (see Section 2 of the main text). Panels *e-h* present observational data for selected stations within each ocean basin for comparison.

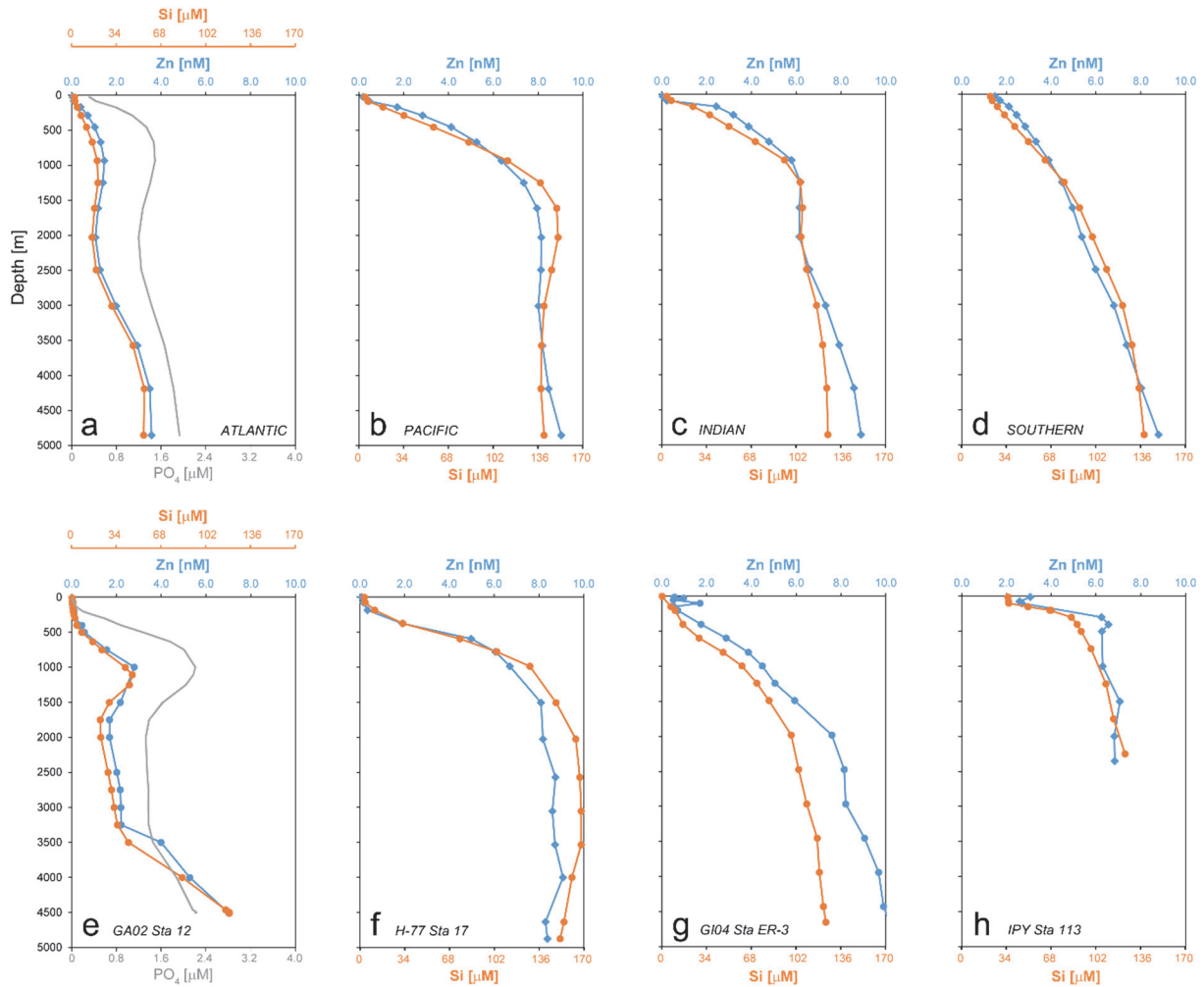


Fig. 4: Maps of (a,b) surface Zn concentration and (c,d) Zn:PO₄ uptake ratio in simulation G10 (left panels) and G11 (right panels). Simulation G10 is less skilful at reproducing the observed Zn-Si relationship than simulation G11 (Fig. 2), reflected e.g. by the elevation of surface Zn concentrations in the eastern equatorial Pacific Ocean (panel *a*). Panel *c* shows the relatively low Zn:PO₄ uptake ratios simulated by G10 in the high-latitude oceans, in contrast to the high ratios in simulation G11 (panel *d*).

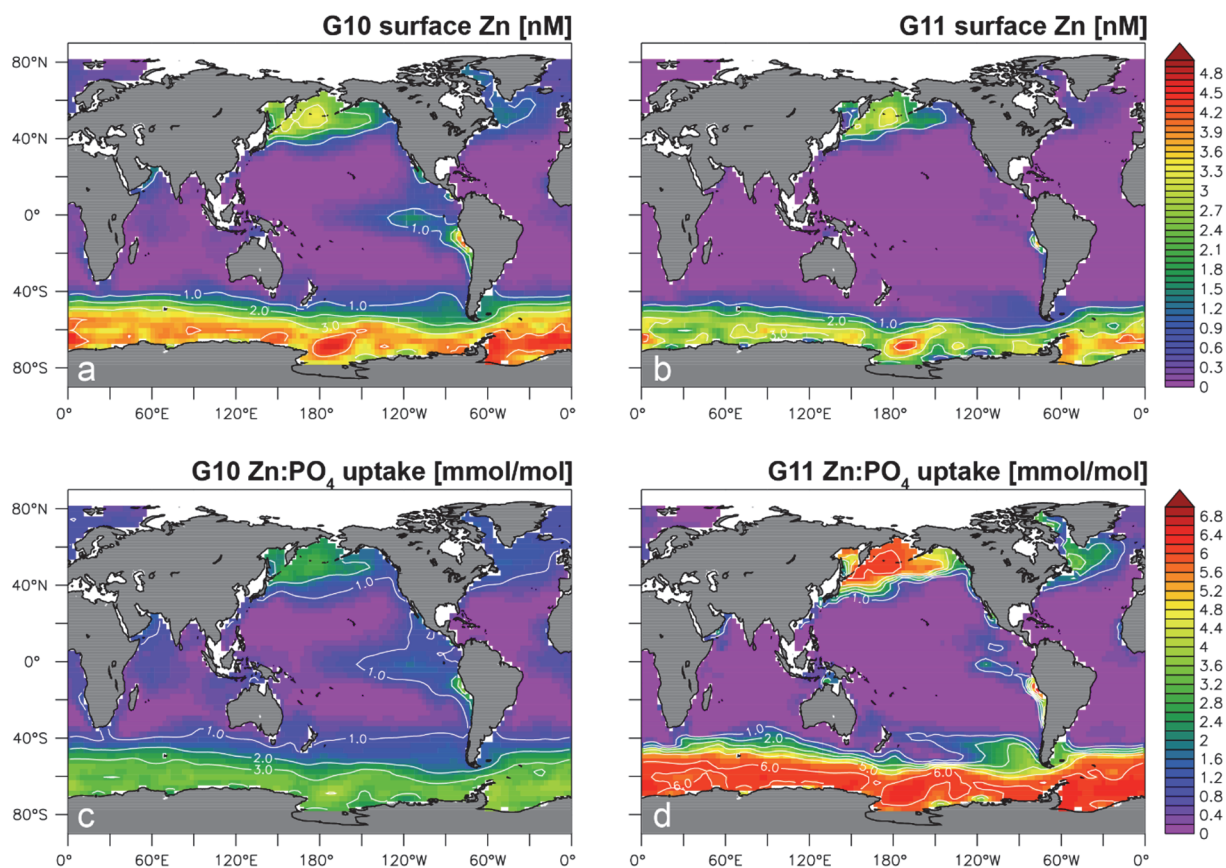


Fig. 5: Maps of Zn:PO_4 uptake ratios in simulations G21-G24, illustrating the effects of varying parameters a_{Zn} and c_{Zn} of Eqn. 1. It can be seen that whilst a high c_{Zn} -value can lead to elevated uptake at high latitudes (panels *a,b*), only a high a_{Zn} -value produces a step-like increase in the Subantarctic Ocean (panels *c,d*). The Subantarctic Zone is indicated by white stippling.

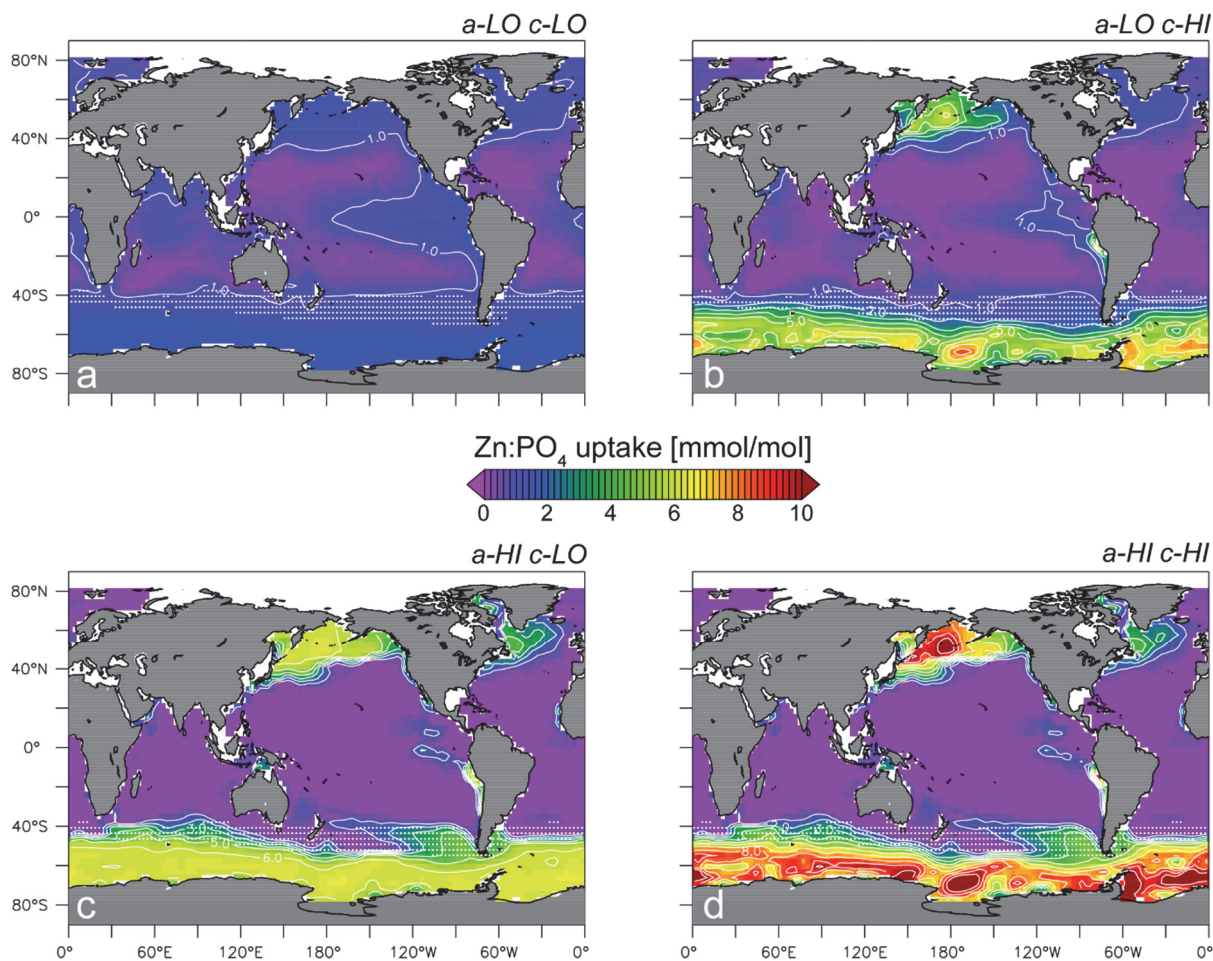


Fig. 6: Zonal average surface Zn concentrations simulated in G21-G24, in which the values of parameters a_{Zn} and c_{Zn} of Eqn. 1 are systematically varied. Dashed grey lines represent two endmember behaviours in which Zn behaves exactly like either PO_4 or Si, produced by scaling the simulated surface PO_4 (or Si) distribution by the Zn: PO_4 (or Zn:Si) ratio of the oceanic inventories. The difference between simulation *aHI-cLO* and *aLO-cLO* shows the influence of elevated values of a_{Zn} on the surface Zn distribution, resulting in a decrease of Zn concentrations in the Subantarctic Zone (~40-50°S) to low values and a poleward migration of the meridional Zn gradients between the high- and mid-latitudes.

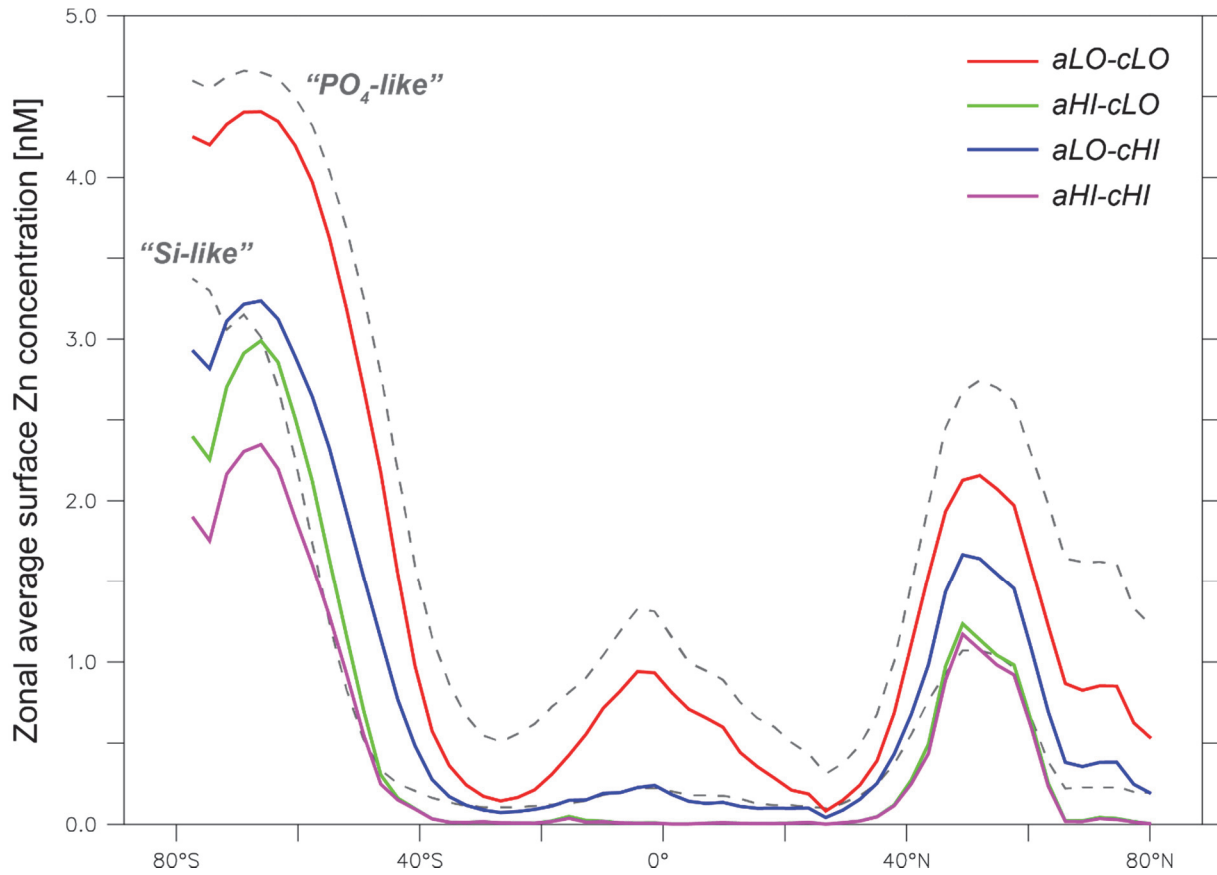


Fig. 7: Sensitivity simulation systematics in (a,b) the CYCLOPS 18-box model and (c,d) MITgcm-2.8 OGCM simulations (G1-G11,G21-G24). Panels *a* and *c* show that higher Southern Ocean Zn:PO₄ uptake results in a steady decrease in Zn:Si in Subantarctic waters, with values approaching the global ocean mean (blue line) when Southern Ocean Zn:PO₄ uptake is around 5 mmol/mol. Panels *b* and *d* show metrics for the similarity between the resulting Zn and Si tracer fields (correlation coefficient r^2 or normalised root-mean-square difference \hat{E}). These metrics show that as the surface Subantarctic Zn:Si approaches the global mean, the similarity between the simulated Zn and Si tracer fields is at their highest, as reflected by high values of r^2 in panel *b* and low \hat{E} in panel *d* (note the reversed y-axis).

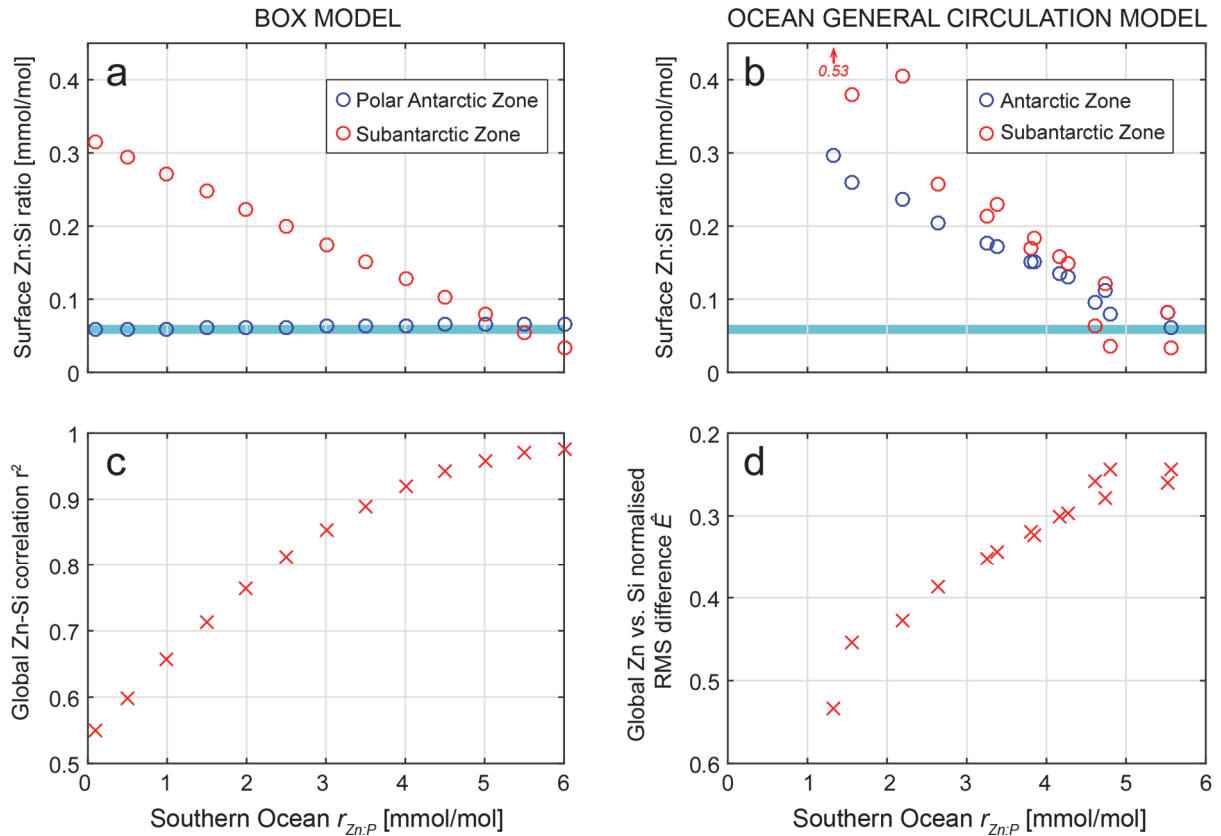


Fig. 8: Surface maps of the Zn:Si ratio in the two simulations presented in Fig. 4. Unlike simulation G10 (panel *a*), in which there is a strong increase in the Zn:Si ratio from the Antarctic to the Subantarctic zone, the surface Southern Ocean has a relatively homogeneous Zn:Si ratio in the simulation G11 (panel *b*), close to the mean-ocean ratio of ~ 0.06 mmol/mol. The Subantarctic Zone is indicated by white stippling.

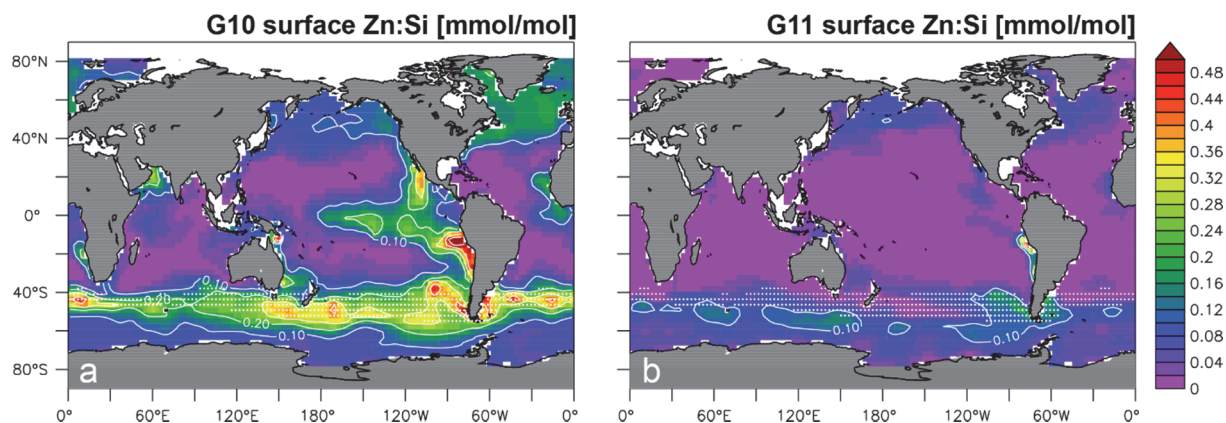


Fig. 9: Systematics of relative Zn and PO₄ drawdown produced by the parameter choices for Eqn. 1 in the OGCM sensitivity simulations. Panels *a* and *c* show the residual Zn as a function of residual PO₄, whilst panels *b* and *d* show the $r_{Zn:P}$ uptake ratios that lead to this relationship. Red circles represent observations in the surface Southern Ocean along the prime meridian by Zhao et al. (2014), normalised to the maximum concentrations of Zn and PO₄ observed along the section (3.7 nM and 1.85 μ M respectively) at the Antarctic Divergence. These values were also used as the initial conditions for the calculation of Zn drawdown using Eqn. 1. Note the close correspondence between the degree of drawdown of Zn and model skill at reproducing the global Zn-Si relationship (cf. Fig. 2).

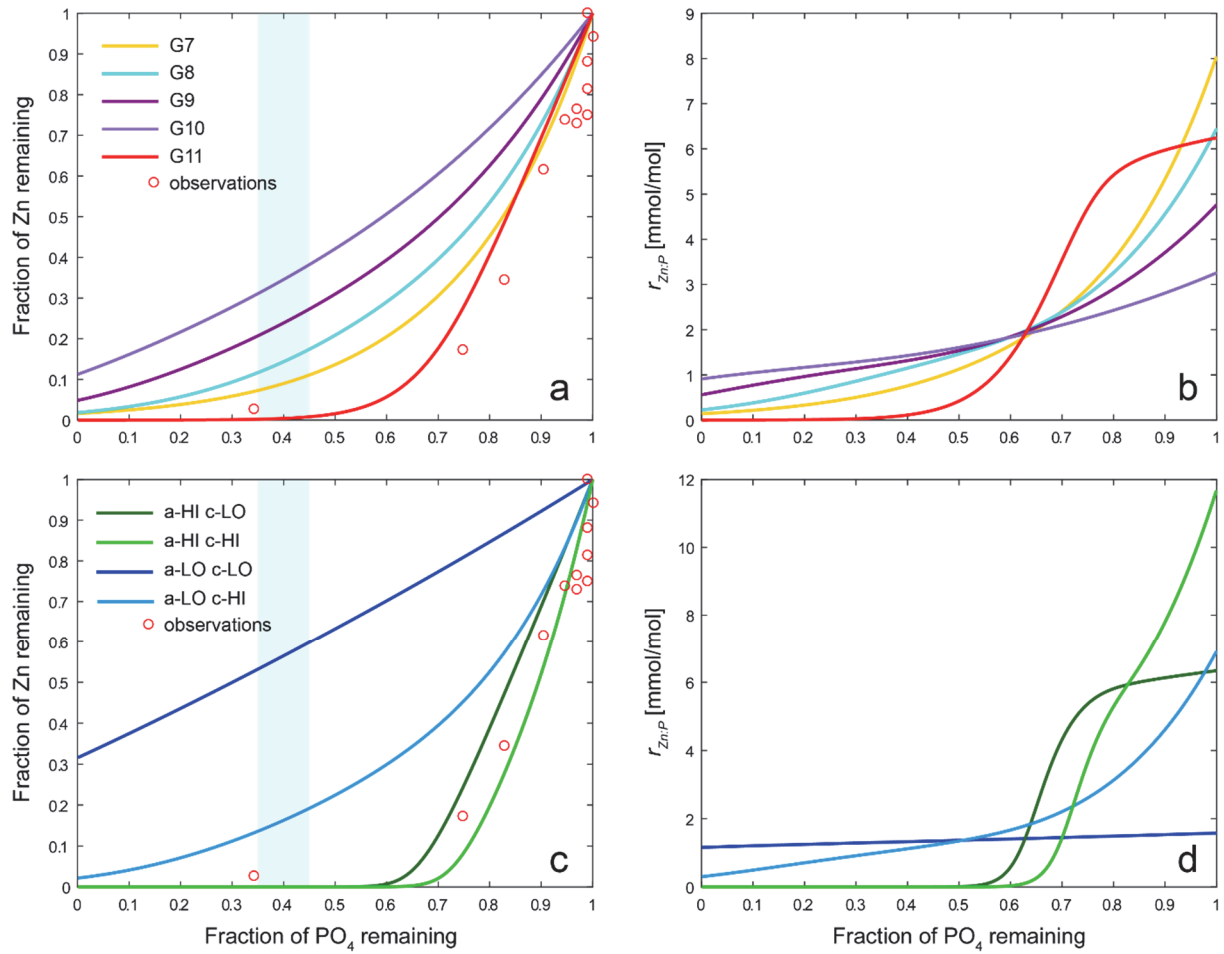


Fig. 10: Cartoon illustrating a potential mechanism for Subantarctic control of global marine elemental correlations. If element Y is more strongly depleted than element X in the Subantarctic Zone relative to their mean-ocean ratio, the low-concentration endmember subducted into the interior from the Subantarctic will lie below the line connecting the deep ocean and the origin (orange diamond). Circulation and mixing of these upper-ocean water masses will produce the concave-upward relationship seen e.g. between Zn and PO_4 in the global ocean. The blue diamond represents the case in which both elements are present in approximately their global-ocean mean ratio in upper-ocean waters subducted from the Subantarctic, leading to a close-to-linear relationship at the global scale, as for Zn and Si .

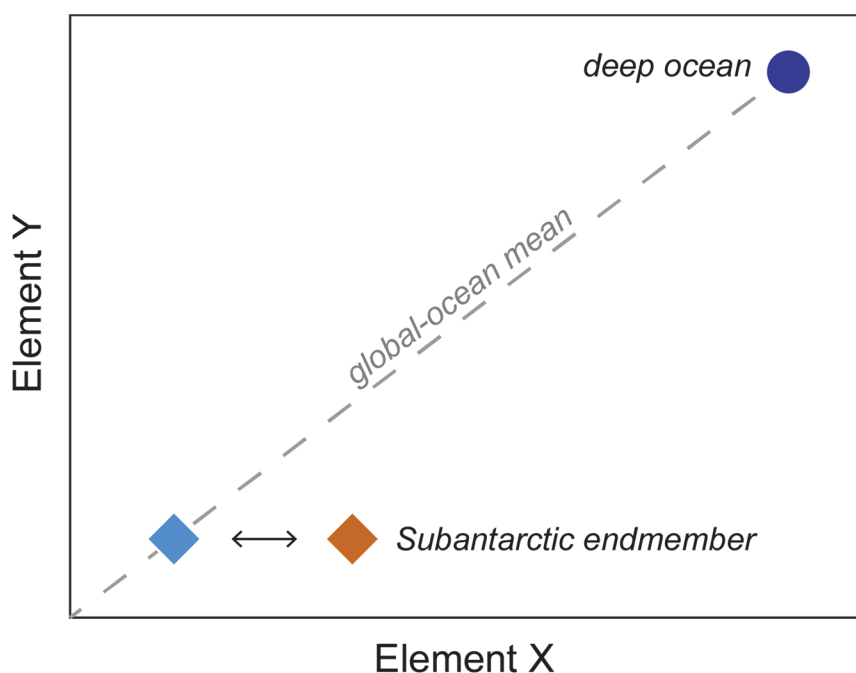


Table 1: Parameter values and brief description of OGCM simulations performed for this study.

Simulation	Model variant	Description	Key parameter values			\hat{E}'	
			m_{Zn} [mol:mol/ μ M]			vs. Si	vs. PO ₄
G1	LIN	0.25 \times standard slope		0.339		0.53	0.16
G2	LIN	0.5 standard slope		0.679		0.43	0.37
G3	LIN	Standard slope (Eqn. 1 fit to <i>T. oceanica</i>)		1.357		0.34	0.59
G4	LIN	1.5 \times standard slope		2.036		0.30	0.70
G5	LIN	2 \times standard slope		2.714		0.27	0.77
G6	LIN	3 \times standard slope		4.071		0.26	0.86
			a_{Zn} [mol:mol]	b_{Zn} [μ M]	c_{Zn} [mol:mol/ μ M]		
G7	NONLIN	Eqn. 3 fit to <i>E. huxleyi</i> A1383	2.4×10^{-3}	4.0×10^{-5}	4.7	0.30	0.71
G8	NONLIN	Eqn. 3 fit to <i>T. weissflogii</i>	1.6×10^{-3}	1.7×10^{-5}	4.0	0.32	0.66
G9	NONLIN	Eqn. 3 fit to <i>T. oceanica</i>	1.25×10^{-3}	1.0×10^{-5}	2.9	0.35	0.6
G10	NONLIN	Eqn. 3 fit to <i>T. pseudonana</i>	1.2×10^{-3}	8.0×10^{-6}	1.7	0.39	0.52
G11	NONLIN	Eqn. 3 fit to <i>E. huxleyi</i> BT6	6.0×10^{-3}	3.0×10^{-5}	0.32	0.26	0.81
G12	NONLIN	<i>aLO</i>	1.2×10^{-3}	1.0×10^{-5}	2.9		
G13	NONLIN	<i>aMID</i>	2.4×10^{-3}	1.0×10^{-5}	2.9		
G14	NONLIN	<i>aHI</i>	6.0×10^{-3}	1.0×10^{-5}	2.9		
G15	NONLIN	<i>bLO</i>	1.25×10^{-3}	8.0×10^{-6}	2.9		
G16	NONLIN	<i>bMID</i>	1.25×10^{-3}	3.0×10^{-5}	2.9		
G17	NONLIN	<i>bHI</i>	1.25×10^{-3}	4.0×10^{-5}	2.9		
G18	NONLIN	<i>cLO</i>	1.25×10^{-3}	1.0×10^{-5}	0.32		
G19	NONLIN	<i>cMID</i>	1.25×10^{-3}	1.0×10^{-5}	1.7		
G20	NONLIN	<i>cHI</i>	1.25×10^{-3}	1.0×10^{-5}	4.7		
G21	NONLIN	<i>aLO-cLO</i>	1.2×10^{-3}	1.0×10^{-5}	0.32		
G22	NONLIN	<i>aHI-cLO</i>	6.0×10^{-3}	1.0×10^{-5}	0.32		
G23	NONLIN	<i>aLO-cHI</i>	1.2×10^{-3}	1.0×10^{-5}	4.7		
G24	NONLIN	<i>aHI-cHI</i>	6.0×10^{-3}	1.0×10^{-5}	4.7		

